

Scheduling Lattice Surgery with Magic State Cultivation

Steven Hofmeyr*, Mathias Weiden†, Justin Kalloor†, John Kubiatowicz†, Costin Iancu*

*Lawrence Berkeley National Laboratory

†University of California, Berkeley

Abstract—Fault-tolerant quantum computation using surface codes relies on efficient scheduling of non-Clifford operations, realized via the injection of magic states produced through a probabilistic process that dominates spacetime costs. Existing scheduling approaches use dedicated bus qubits for routing and separate peripheral ancilla qubit factories for magic state preparation, leading to inefficient resource utilization. With the advent of magic state cultivation, preparation qubits can be placed anywhere within the surface code architecture. We introduce Pure Magic scheduling, which dynamically re-purposes magic state cultivation qubits for routing operations, eliminating dedicated bus infrastructure. By interrupting cultivation when qubits are needed for routing, Pure Magic naturally favors shorter cultivation times while ensuring no ancilla qubit remains idle. Our evaluation across 17 benchmark circuits improves scheduling efficiency by 19% to 223% compared to traditional bus routing and decreases average magic state preparation time by $2.6\times$ to $9.7\times$. Benefits scale with circuit parallelism, making Pure Magic particularly valuable for highly parallel quantum algorithms. The Pure Magic architecture represents a paradigm shift from static to dynamic, demand-driven scheduling in fault-tolerant quantum architectures.

I. INTRODUCTION

The immense potential of quantum computing is tempered by the high error rates observed in existing hardware. As a result, scalable architectures must rely on Quantum Error Correction Codes (QECCs), which encode fewer logical qubits into many physical qubits to detect and correct errors. The surface code [8], [13] is a widely studied QECC because it requires only nearest-neighbor interactions on a two-dimensional grid, making it especially well-suited to hardware that provides planar connectivity between physical qubits (e.g. superconducting qubits). Long-range interactions between logical qubits are provided via lattice surgery, the dynamic merging and splitting of code patches using targeted measurements and hardware manipulations [12].

Surface codes face a fundamental challenge: they cannot directly implement arbitrary quantum gates. Instead, they rely on a restricted set of operations supplemented by *magic states*, which are specially prepared quantum states that enable universal computation [3]. Magic state preparation has historically required distillation protocols that consume thousands of noisy auxiliary states to produce a single high-fidelity magic state, creating enormous resource overhead [7].

The execution of a high-level quantum circuit on a target QECC such as a surface code employs a compiler to transform a sequence of single- and two-qubit interactions

into multi-qubit Pauli product measurements for Pauli Basis Computation [4], [19]. The goal of the compiler is to minimize the space (qubits) and time (logical cycles) of the compiled program. Doing so efficiently requires managing the additional logical qubits needed for routing long-distance operations and preparing magic state. To address this challenge, existing surface-code architectures assign fixed roles to different regions of the grid: *data* qubits store program state, *bus* qubits enable routing via lattice surgery, and dedicated *magic* patches produce magic states. These designs typically assume large, space-intensive magic-state distillation factories [3] placed statically along the grid boundary.

As an alternative to distillation, recent work has introduced magic-state cultivation, a more resource-efficient method that prepares a magic state using the footprint of only a single logical qubit [10]. Using cultivation, magic state production can be assigned to any qubit, not just those on the grid boundary. This enables a new approach, which we call *Pure Magic*: a dynamic lattice surgery scheduling approach that repurposes qubits on demand. In this approach, there are only data and ancilla qubits. Ancillae continuously cultivate magic states, and when an ancilla qubit is needed for routing, cultivation is canceled. After routing, the cultivation process restarts immediately.

We implement the Pure Magic approach through a new scheduler, which determines the order in which to execute a sequence of Pauli products comprising a circuit. Many of these Pauli products can be simultaneously executed on the surface code, given adequate routing and magic state resources. Determining how to order the execution to maximize parallelism is the Lattice Surgery Scheduling Problem (LSSP), which can be solved by a greedy Steiner tree packing algorithm [25].

We evaluate the Pure Magic scheduler on benchmarks from Benchpress [21], augmented with randomly generated circuits. Across these tests, Pure Magic reduces scheduling volume—a proxy for execution time and logical error—by 19% to 220% relative to state-of-the-art techniques. By re-purposing ancilla patches for both routing and cultivation, Pure Magic eliminates dedicated bus qubits and significantly increases the number of active cultivators. Moreover, the dynamic reuse of ancilla patches mitigates the long-tail behavior of probabilistic cultivation: routing frequently interrupts the slowest cultivation attempts. This leads to an effective $2.4\times$ - $6.7\times$ reduction in average cultivation time. These advantages are most pronounced in highly parallel circuits with substantial demand for

magic states. Reducing average magic-state generation time is particularly valuable because the overall speed of a fault-tolerant quantum computer is governed by how quickly magic states can be produced and consumed.

This work makes the following contributions:

- A Pure Magic scheduler with an improved greedy packing algorithm, designed to use cultivation instead of distillation for magic state generation.
- Scheduling mechanisms that explicitly model magic-state injection latency and variability, with analysis of their impact.
- An analysis of compiled circuit structure, motivating new compilation heuristics that better reflect the behavior of real benchmark workloads.

We expect Pure Magic to generalize to other QECCs that rely on magic state injection. Since new codes are often benchmarked against the surface code, Pure Magic provides an additional criterion for comparing QECC efficacy.

II. BACKGROUND

In this section, we cover details pertinent to quantum error correction with two-dimensional (2D) surface codes and the scheduling challenges they present.

A. Surface Codes

The surface code is a 2D topological quantum error-correcting code designed for hardware with only nearest-neighbor interactions. It is the most widely studied QECC because it combines high error thresholds with simple, local operations.

At the physical level, a single logical qubit is encoded as a grid of physical qubits, as shown in Figure 1a. The grid size is characterized by the code distance d . Additional ancilla qubits interact locally with nearby data qubits to measure stabilizers—parity checks that detect errors without collapsing the encoded information. The surface code uses only X and Z stabilizers that measure products of Pauli operators on small neighborhoods of data qubits.

We model surface-code logical qubits as *patches* arranged on a two-dimensional grid [12]. This abstraction ensures that all required physical operations map cleanly onto a planar architecture. The edges of each patch play a central role: merging patches along specific edges performs joint parity measurements of the corresponding logical operators [7], [12]. Figure 1b shows a single surface-code patch with its X - and Z -type edges labeled. In our architecture, we employ *double-qubit patches*, represented as 2×1 rectangles. Each such patch encodes two logical qubits within a single surface-code region. This layout places the X and Z operators for each qubit along the same boundary of the rectangle, enabling more efficient multi-qubit interactions and simplifying lattice-surgery operations (Figure 1c).

B. Pauli Basis Computation via Lattice Surgery

Input circuits are assumed to use the standard Clifford+T gate set [8], [19], [22]. Our compiler transforms Clifford+T

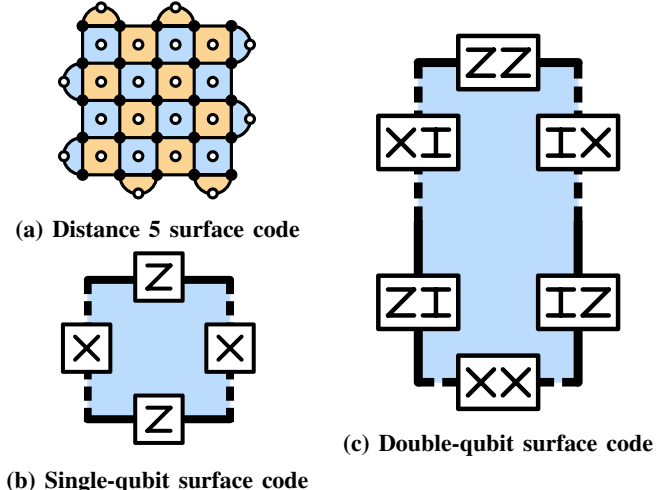


Fig. 1: Representations of surface code logical qubits. (a) A distance 5 surface code storing one logical qubit. Black circles are physical data qubits, white circles are physical ancilla qubits. Blue (orange) squares represent Z (X) stabilizers. (b) Single logical qubit patch with rough (X , dashed) and smooth (Z , solid) edges. This patch represents the same qubit as (a). (c) Double-qubit patch encoding two logical qubits with accessible X/Z operators on both sides. Top (bottom) edges expose joint ZZ (XX) operators.

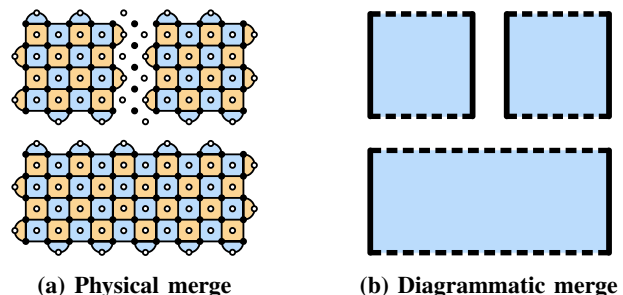


Fig. 2: Smooth (Z type) merge operations. (a) Adjacent patches merge by adding joint stabilizers, then split by measuring bridge qubits. (b) Diagrammatic representation combining Z edges.

circuits into sequences of Pauli product rotations by rewriting gates into their Pauli rotation equivalents (e.g., $S = Z_{\pi/4}$, $T = Z_{\pi/8}$). All Clifford operations are commuted to the end of the circuit and absorbed into measurements using the Clifford tableau method [1], [25].

The resulting circuit consists of *multi-qubit $\pi/8$ Pauli products* that must be scheduled on the chip. Each Pauli product performs the n -qubit unitary $\exp(-P_n\pi/8)$ where $P_n = \bigotimes_{i=1}^n P_i$ and $P_i \in \{X, Y, Z, I\}$.

Lattice surgery [12] provides an efficient method to execute Pauli products through *merge* and *split* operations, as shown in Figure 2. These form the native instruction set of lattice surgery architectures.

A complete Pauli product execution involves three steps:

- 1) Edge selection: For each qubit i in the Pauli product P_n , select edges corresponding to P_i : X operations require X

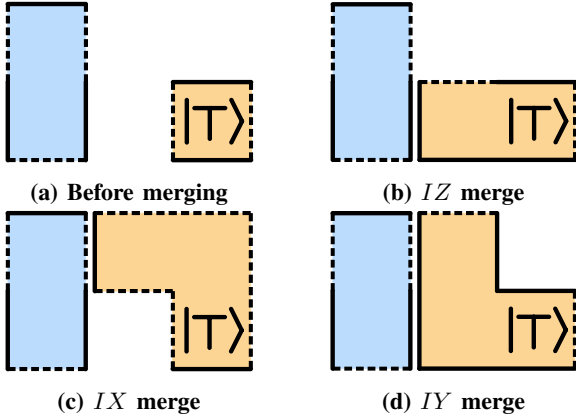


Fig. 3: T state injection via lattice surgery. Magic T states (orange) enable $\pi/8$ rotations of type X , Y , or Z through different merge operations. These primitives are used to implement Pauli products.

edges, Z operations require Z edges, and Y operations require both X and Z edges simultaneously.

- 2) Magic state injection: Merge each selected edge with a magic state qubit's Z edge. This requires finding paths of empty patches to connect the appropriate edges on the grid.
- 3) Measurement: Split the multi-qubit product by measuring connection qubits. The measurement outcome determines any needed Clifford corrections, which can be commuted to the circuit's end.

Executing a Pauli product takes one logical cycle, provided magic states are available and routing paths exist. Figure 3 shows different merge types for various Pauli operations.

C. Magic State Cultivation

Universal quantum computation requires magic states, which cannot be initialized fault-tolerantly. Traditional approaches rely on *distillation*, a process that consumes thousands of noisy resource states to produce a single high-fidelity one, leading to extremely large overheads [3], [8].

Recent work by Gidney et al. [10] introduced *cultivation*, a far more efficient approach using the same physical resources as a single logical qubit. Cultivation proceeds in three stages. First, *injection* creates the initial encoded T state in a low-distance code. Second, *cultivation* gradually increases reliability using “check-grow-stabilize” cycles with post-selection (shots are discarded when any error is detected). Finally, the *escape* stage quickly boosts the code distance to prevent the highly reliable state from degrading. At this point the code is “grafted” into a matchable surface-code-like patch. Cultivation’s efficiency enables more practical algorithm implementations and compact architectures [9], but existing scheduling algorithms have not thoroughly studied its implications for resource management.

D. Other approaches to FTQC with Surface Codes

Prior work on lattice-surgery compilation spans several distinct approaches. *LaSynth* [27] introduces a SAT encoding of

lattice surgery that can produce depth-optimal implementations of small-scale primitives. Although optimal, the method does not scale to the compilation of full application-level circuits. Building on SAT-based formulations, *DASCOT* [20] presents an encoding of the Lattice Surgery Scheduling Problem together with heuristic approximations to optimal solutions; however, it assumes that magic states are always available when needed and operates directly on Clifford+T circuits rather than translating them into Pauli products. Similarly, *liblsqecc* [17] proposes a framework for directly executing Clifford+T gates but considers only earlier generations of magic-state distillation and does not incorporate recent cultivation techniques. An alternative approach uses factory-less distillation layouts with static scheduling to exploit locality [11].

Architectural work has also explored ways of mitigating resource bottlenecks. *LSQCA* [14] introduces a design in which surface-code patches expected to be used soon are kept in sparse compute regions, while others are stored in denser regions; the movement between these regions helps conceal the latency of magic-state generation.

III. SCHEDULING

The goal of the scheduler is to solve the *Lattice Surgery Scheduling Problem* (LSSP). Given a circuit comprised of a sequence of Pauli products with L qubits, the scheduling algorithm must compute an ordering of the Pauli products that minimizes volume, thereby minimizing the probability of error. The scheduler must also determine the grid layout of the logical qubits, with L data qubits and additional ancilla qubits for routing and magic injection, for a total of $N > L$ qubits.

Each Pauli product will take exactly one logical cycle to schedule, and multiple Pauli products that use any of the same qubits cannot be scheduled concurrently. Otherwise independent Pauli products can be scheduled simultaneously. Consequently, the Pauli products form a dependency or task graph, and the goal of the scheduling algorithm is to determine the order in which to execute the task graph. The graph can be visualized in layers, as seen in Figure 4, which shows a slice of a 16-qubit circuit. Different colors indicate different Pauli products, with some layers having multiple Pauli products that can be co-scheduled, while other layers have only one Pauli product.

We use the scheduling *volume* as a proxy for the error rate. For N logical qubits and T logical execution cycles, the volume is $V = N \times T$. We assume an error model:

$$P(\text{error}) = P_L \times N \times T \quad (1)$$

P_L is the error rate for a single logical qubit, and is typically modeled as:

$$P_L \propto (\epsilon/\epsilon_{th})^{(d+1)/2} \quad (2)$$

Here ϵ is the error rate per physical qubit per cycle, ϵ_{th} is the error threshold, and d is the code distance. Equation 1 assumes that physical errors (e.g. bit-flips, phase flips) are independent and identically distributed, both in time and space. In practice the error rate can be much more complex with

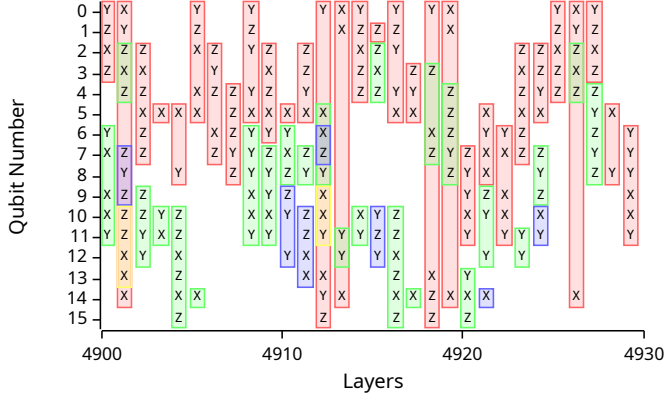


Fig. 4: A sequence of Pauli products taken from a benchmark circuit. Each product is represented by a different color rectangle, and the operators that are assigned to qubits are indicated by the X , Y and Z letters. Products shown in the same layer (vertical column) are eligible for co-scheduling.

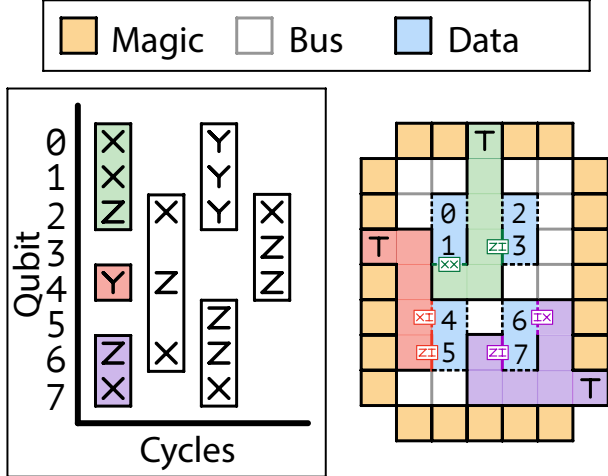


Fig. 5: A bus routing architecture with eight data qubits (blue), 27 bus qubits (white, red, green, and purple) and 24 magic qubits (orange). Also shown are three products scheduled on the layout: the double XX in the green product can be connected to the bottom of the 0/1 double qubit. Other single X and Z values must connect to the sides of their target data qubits. The Y operator in the red product must connect to both a X and Z on the side of the 4/5 data qubit.

dependent effects, governed by the underlying hardware. We follow other analyses in this area [8], [23] and use the simple error model. Minimizing volume minimizes errors under this error model.

A. Layouts

A layout is a placement of logical qubits on a 2D grid. The exposed X and Z edges of each logical qubit correspond to logical operators that can be merged through lattice surgery

(Figure 3). We model these surgery operations as paths on a grid. An example of such a grid is given in Figure 5, where qubits are represented by rectangular patches, and the connections are made to patch edges that correspond to a given Pauli operator. The state-of-the-art *bus routing* grid contains three types of patches: *data* (blue), *bus* (white), and *magic* (orange).

Scheduling a Pauli product on the bus routing layout requires connecting the relevant edges through available bus qubits and ultimately terminating the path at a magic patch. A Y Pauli measurement must connect to both the X and Z edges of that logical qubit (as illustrated in Figure 3d). The resulting Pauli product operation forms a tree on the grid whose leaves correspond to the Pauli operators and include one magic state.

Connectivity constraints arise from the structure of the double-qubit patches. Bus and magic squares can be connected on all four edges, but data qubits are restricted: each double-qubit can be connected either from a single side or simultaneously from both its top and bottom edges. An example of three scheduled Pauli products is illustrated in Figure 5. The logical operators Z_2 , Y_4 , Z_6 , and X_7 are connected via the sides of the rectangular data qubits. A bottom edge is used for the 0/1 double qubit to perform a X_0X_1 measurement. The Y term connects to both the X and Z edges of the logical qubit 4, i.e. $Y_4 = X_4 \times Z_4$.

B. Magic Injection Using Cultivation

Executing a non-Clifford ($\pi/8$) product requires a magic state, which is represented by a magic patch in the layout grid. We assume that magic states can be produced through cultivation (as described in Section II-C), hence only a single grid patch is required to cultivate one magic state qubit. We model the time taken to cultivate the magic state using an exponential distribution:

$$E(T) = \lambda e^{-\lambda x} \quad (3)$$

We conducted Markov Chain Monte Carlo (MCMC) simulations using the survivorship probabilities of each stage of magic state cultivation outlined in Figure 15 of Gidney et. al. [10]. We simulated the cultivation of fault-distance-3 magic states so as to attain an error probability of $p_L \approx 4 \times 10^{-6}$. Fitting the simulation data to Equation 3 yields a value of $\lambda = 0.00227$. The duration of cultivation in scheduling cycles can be computed by taking samples from this exponential distribution then dividing by the code distance. Figure 6 shows the cumulative distribution function of 10^6 simulated runs of cultivation.

The relationship between noise model, intermediate fault-distance, and final code distance is highly complex. Furthermore, recent work has demonstrated how cultivation can be made more time efficient [24], [28]. For this reason, we match the parameters presented in Figure 15a of Gidney et. al. [10], but leave λ as a controllable hyperparameter of our simulation framework.

When a magic state is ready, it can be used to schedule a Pauli product. In the cycle following the scheduling, the magic

state qubit will restart cultivation, and hence will likely only be ready several cycles in the future.

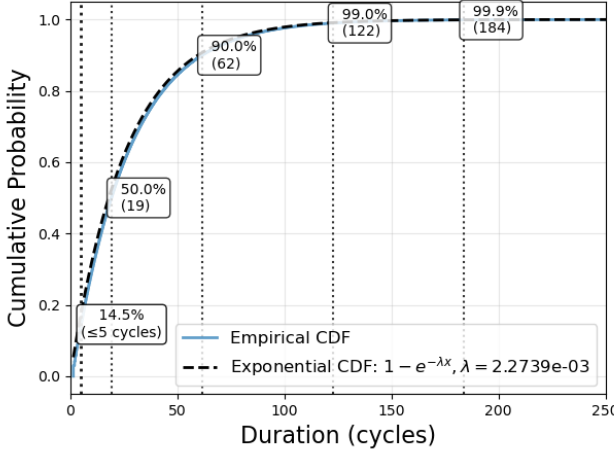


Fig. 6: Cumulative distribution function for simulated T state cultivation. The median cultivation time is approximately 19 cycles, but 14.5% of cultivation trials take 5 or fewer cycles. The empirical CDF consists of 10^6 simulated runs. Our simulations assume a final matchable surface code distance of 17.

C. Packing Steiner Forests

The scheduling algorithm attempts to maximize the number of non-overlapping, independent Pauli products scheduled in each cycle. As described previously, each Pauli product is scheduled as a tree on the grid. Ideally this is a Steiner tree, which connects all the *terminals* (the set of leaves representing the Pauli product operators) via the shortest paths. However, finding a Steiner tree is in general an NP-hard problem [18] so we find approximate Steiner trees using a variant of the shortest path heuristic [15]. This yields a tree with weight (path length) within $2 - 2/S$ of the Steiner tree, where S is the number of terminals. Although there are other algorithms with improved lower bounds on the approximation, in practice the shortest path heuristic provides sufficient accuracy for the sizes of trees for typical circuits.

Maximizing the number of simultaneously scheduled Pauli products is akin to solving the Steiner forest packing problem [16], which is also NP-hard. We find an approximate solution with a greedy *MINFIT* algorithm, as shown in Algorithm 1. The algorithm begins with the set of available Pauli products (those that have no parents in the task graph) and all squares in the grid. In each iteration of the while loop (line 4), for every Pauli product an approximate Steiner tree is calculated for the available patches (line 6), and the Pauli product with the shorter path (the *minimum fit*) is chosen as the next to schedule (lines 7 to 10). That Pauli product is added to the Pauli products to schedule next (line 12), and removed from the list of available Pauli products (line 13), while the patches used by the tree for the Pauli product are removed from the available patches (line 14). Once all

available Pauli products have been attempted, the cycle is complete. The *MINFIT* algorithm is repeated every cycle until no more unscheduled Pauli products remain, resulting in a schedule that indicates which Pauli products are to be executed at each cycle.

Algorithm 1 Greedy MINFIT Steiner forest packing algorithm

```

1: avail_products  $\leftarrow$  products with no dependencies
2: avail_patches  $\leftarrow$  all patches in layout grid
3: scheduled_products  $\leftarrow$   $\emptyset$ 
4: while avail_products is not empty do
5:   for each product in avail_products do
6:     tree  $\leftarrow$  FindSteinerTree(product, avail_patches)
7:     if tree is valid and tree  $<$  min_tree then
8:       min_tree  $\leftarrow$  tree
9:       min_product  $\leftarrow$  product
10:      end if
11:    end for
12:    add min_product to scheduled_products
13:    remove min_product from avail_products
14:    remove patches in min_tree from avail_patches
15:  end while
16:  return scheduled_products

```

IV. PURE MAGIC SCHEDULING

One of the most significant performance constraints in surface-code quantum computation is the production of magic states. Even with cultivation, T-state preparation remains slow. Using the parameters reported in Gidney et. al. [10], our simulations indicate an average cultivation time of roughly 26 logical cycles. The latency of cultivation remains a large source of run time overhead, which is detrimental to performance for near-term architectures.

A key observation is that cultivation does not require dedicated, long-lived cultivator patches. Cultivation can be terminated and restarted at any time. This flexibility allows us to repurpose the mostly idle bus qubits traditionally reserved for routing as additional cultivators. Doing so transforms the layout as shown in Figure 7: dedicated bus patches disappear, and all ancilla patches become dual-purpose regions capable of both cultivation and routing.

Scheduling proceeds as follows. To execute a Pauli product, the scheduler forms a Steiner tree connecting the required data-qubit operators using whatever magic patches are currently available as routing intermediates, canceling any cultivation in progress. Once a patch is no longer needed for routing, it immediately restarts cultivation. This ensures that (1) Steiner trees can still be formed for every Pauli product, and (2) no ancilla qubit is ever idle—every non-data patch is cultivating whenever it is not actively routing. We refer to this design as the *Pure Magic* architecture.

Figure 8 shows how three Pauli products are scheduled onto the two layouts. Each product is shown by patches merged through lattice surgery, with the routing patches corresponding to the product color (green, red, purple). The ready magic state

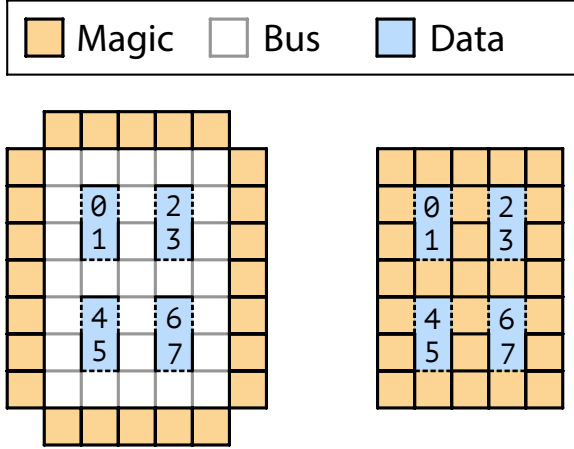


Fig. 7: Comparison of architectures for eight logical data qubits. Double surface code patches each encode two logical qubits. Whereas the bus routing layout uses dedicated bus qubits (white patches), the Pure Magic layout, uses all ancilla qubits for both cultivation and routing (orange patches). The Pure Magic layout requires fewer overall qubits to ensure full access to all data qubits.

used is indicated by the label T. In the case of bus routing, the merged routing patches are comprised of dedicated bus qubits, whereas for Pure Magic scheduling, they are comprised of magic patches repurposed for routing. In bus routing, the magic state used in a product is always on the periphery, whereas it can be anywhere for Pure Magic scheduling, resulting in reductions in the tree sizes of scheduled products (e.g. the green product uses 6 routing patches in bus routing, and only 4 in Pure Magic scheduling).

In the Pure Magic approach, all ancilla patches not involved in the product scheduling continue to cultivate magic state. This approach both increases the rate of magic state cultivation and reduces the minimum number of additional qubits required to schedule a circuit. The number of simultaneously cultivating surface code patches no longer scales with the *perimeter* of the chip (as in bus routing on distillation-factory architectures), but instead with the entire ancillary *area* of the layout. This decoupling is particularly pronounced for 2D surface code architectures, where the perimeter grows only as $O(\sqrt{N})$ while the area grows as $O(N)$.

Another advantage of the Pure Magic approach is that it addresses the issue with the long-tailed exponential distribution of magic state cultivation, where a magic qubit could potentially take hundreds of cycles to cultivate a T state, resulting in wasted resources. With Pure Magic scheduling, long running cultivation is likely to be terminated by routing, and the most rapid cultivation attempts are favored.

V. EXPERIMENTAL RESULTS

The schedulers for bus routing and Pure Magic routing are implemented in the Rust programming language and the code

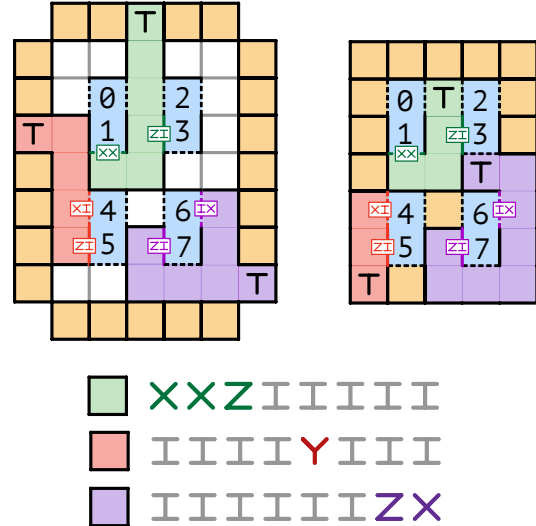


Fig. 8: Simultaneously scheduling three Pauli products on a bus routing layout vs. a Pure Magic layout. The green, red, and purple colored patches represent the scheduled Pauli products. The operators measured (e.g. XX , IZ , etc.) as part of each Pauli product are labeled on the data qubit that they effect. The logical qubits with ready magic states used to implement the Pauli products are labeled with T.

is freely available and open source¹. We investigated many aspects of scheduler performance, as detailed in this section.

A. Test Circuits

We used a set of 17 benchmark circuits drawn from the Benchpress² quantum circuit suite [21], as shown in Table I. These circuits span many domains of interest (Quantum Machine Learning, Ising Models, Heisenberg Models, Convex Optimization). The circuits were lowered from their initial gate set to the standard Clifford+T gateset using BQSKit [2]. Clifford+T circuits were then converted to a sequence of Pauli products using the algorithm described in Silva et. al. [25]. The layers are derived from the task graph of the resulting Pauli products.

As Clifford+T gates are not being executed directly, we consider the *parallelism* of the circuit as the average number of Pauli products per layer. Scheduling efficiency depends on the Pauli structure, so we include the parallelism of each circuit in Table I. This value ranges from 1.0 (Hubbard 18 qubits) to 33.16 (Ising 98 qubits).

The parallelism of a circuit typically changes over the layers in the task graph. Figure 9 shows an example of how the average Pauli products per layer and Pauli product sizes change for the Heisenberg 16 circuit. The y-values are computed over a moving window of size 100, taking the maximum y in the interval for maximums, and the average y in the interval for the averages. Usually an increase in

¹URL redacted for anonymous review.

²The “Heisenberg” benchmarks are the “Square Heisenberg” in the Benchpress repository.

TABLE I: Characteristics of quantum circuits used for experimental evaluation.

Circuit	Qubits	Gates	T gates	Layers	Products/layer	
					Avg.	Max.
DNN	8	1018	30822	22140	1.39	7
DNN	16	2034	61210	26293	2.33	13
DNN	51	518	125315	71422	1.76	51
Heisenberg	16	1025	45994	28898	1.59	16
Heisenberg	36	2557	113454	63176	1.80	36
Heisenberg	64	4769	212276	110381	1.92	64
Heisenberg	144	11233	497672	246537	2.02	144
Hubbard	18	21874	244836	243995	1.00	5
Ising	26	310	9430	960	9.85	24
Ising	66	790	25420	1174	21.71	47
Ising	98	1174	36914	1116	33.16	69
KNN	25	41	32391	19082	1.70	25
KNN	129	197	171849	109354	1.57	129
QAOA	36	793	52274	41492	1.26	6
QAOA	149	3392	223154	171063	1.31	78
QFT	63	9895	367533	340088	1.08	51
QV	36	27865	992494	891102	1.11	27

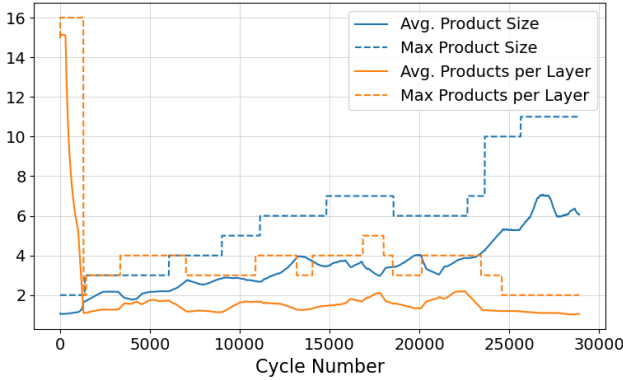


Fig. 9: Cross layer characteristics of Heisenberg 16 circuit expressed using Pauli products. The averages are computed over a moving window of size 100, and the maximums are computed as the largest value of that same moving window.

parallelism corresponds to a decrease in Pauli product size, as smaller Pauli products are less likely to overlap in qubits. Because circuits can exhibit phases, future versions of Pure Magic scheduling may work to change scheduling strategy over the course of the execution.

B. Improvements from Pure Magic Scheduling

We compare the performance of the Pure Magic scheduling approach to bus routing in Table II. Each result is the median of 10 runs. The variance in logical cycles across all benchmarks was less than 2%, which is due to random variations in the cultivation times. We are using the layout shown in Figure 7. We focus on the scheduled *volume* (the total number of logical qubits in the layout multiplied by the logical cycles), using it as a proxy for the error rate, as described in Section III. The *scheduling efficiency* shown in the table is the volume that would be attained on the Pure Magic layout with full parallelism, divided by the actual volume from the schedule. Full parallelism means that all products in a layer can be co-

scheduled in the same cycle, i.e. the number of cycles would be the same as the number of layers in the task graph.

For this set of benchmarks, Pure Magic scheduling improves on the scheduling efficiency by 19% to 223%, and achieves close to maximum efficiency (1.0) on several benchmarks (e.g. QFT). In general, the greater the parallelism in the circuit, the larger the improvement. This is expected because the critical bottleneck for higher parallelism is magic state cultivation, and Pure Magic scheduling provides more resources for cultivation.

A consequence of using magic cultivating qubits for routing is that we tend to favor short-running cultivation processes. This translates into a reduction in the average time taken to cultivate a magic state, as seen in the right-most columns in Table I. As expected from Equation 3, the average cycles taken for bus routing are about 26, whereas for Pure Magic scheduling, they vary from 2.67 to 10.09. In reality, the cultivation process produces a long-tailed distribution, with the result that there is a small chance that cultivation could take an extremely long time, resulting in wasted resources in the bus routing scheme.

TABLE II: Comparison of Pure Magic vs bus routing scheduling performance. The averages for cultivation are computed over the number of cycles magic qubits take to become ready; those terminated before cultivation is ready are not counted.

Circuit	Scheduling Efficiency		% Imprv. Pure Magic	Avg. Magic Cultivation	
	Bus	Pure		Bus	Pure
DNN 8	0.366	0.581	59	26.13	4.50
DNN 16	0.319	0.580	82	26.23	4.50
DNN 51	0.671	0.936	39	26.26	8.02
Heisenberg 16	0.450	0.807	79	26.17	8.08
Heisenberg 36	0.590	0.918	56	26.27	6.88
Heisenberg 64	0.663	0.913	38	26.28	6.60
Heisenberg 144	0.793	0.976	23	26.26	5.29
Hubbard 18	0.657	0.997	52	26.28	6.81
Ising 26	0.122	0.278	128	26.02	7.65
Ising 66	0.091	0.248	173	26.00	6.48
Ising 98	0.069	0.223	223	26.17	5.88
KNN 25	0.552	0.876	59	26.10	10.09
KNN 129	0.726	0.950	31	26.24	8.45
QAOA 36	0.675	0.962	43	26.18	5.81
QAOA 149	0.823	0.980	19	26.26	4.87
QFT 63	0.769	0.998	30	26.26	3.54
QV 36	0.685	0.964	41	26.27	2.67

Because Pure Magic scheduling does not require separate qubits for routing, it uses fewer qubits than bus routing to schedule circuits. This improvement in resource usage (reduction in qubits) can be seen in Figure 10. The percentage improvement for Pure Magic in space (the reduction in qubits) can be seen in the blue crosses. As the number of data qubits increases, the relative advantage gained by the compression of the layout with Pure Magic decreases. The advantage scales inversely with \sqrt{N} , where N is the number of data qubits, because double-qubits are laid out in as close to a square as possible, and bus routing requires an additional perimeter of magic state qubits. This inverse scaling is shown with the

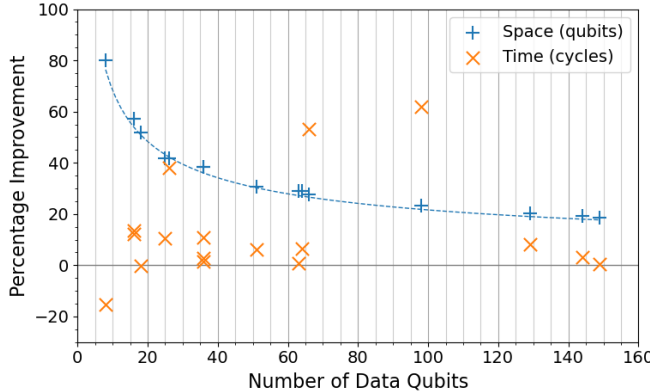


Fig. 10: Relationships between data qubits and improvements in resource usage (qubits and cycles) for Pure Magic scheduling compared to bus routing. The blue crosses show the reduction in total qubits used for the layout, including all data, bus and magic. The orange crosses show the improvement in cycles taken for the schedule. Improvements in Pure Magic volume are not fully explained by reductions made in space due to the architecture’s improved compactness.

dotted blue line, which is fitted to α/\sqrt{N} with an appropriate value (216) for the constant α .

Although the reduction in space (total qubits) is responsible for some of the scheduling efficiency gains for Pure Magic, we also see gains from improved time usage (reduced cycles). This is shown in Figure 10 as the orange crosses, where all of the points (except for 8 data qubits) are above 0%. In cases of high parallelism (e.g. the Ising benchmarks at 26, 66 and 98 qubits), the time improvement is much greater because more ready magic is available. This aspect is explored further in the following section (V-C). In the case of the 8 qubit circuit, we see a 25% drop in time improvement, i.e. the Pure Magic takes more cycles than bus routing. This can be attributed to the fact that for such a small layout, bus routing adds almost as many perimeter magic qubits (24) as there are bus qubits (27). So Pure Magic effectively has fewer magic qubits because it only has 27 for both routing and magic. However, this loss of cycle efficiency is more than compensated for by the improvement in space efficiency at 8 qubits, yielding an overall efficiency improvement of 47%.

C. Tests with Random Circuits

To explore the impact of circuit parallelism on scheduling, we generated a set of random circuits with a wider range of average Pauli products per layer than is present in the benchmarks in Table I. There are many ways of generating random circuits. We used a simple approach where Pauli products were generated with a random size and qubit spread, parameterized to generate larger or smaller Pauli products. To create a random circuit, Pauli products were generated until the required number was reached (20,000 for this publication), and then a task graph was computed as normal. For the results reported here, we focus on random circuits of 64 qubits.

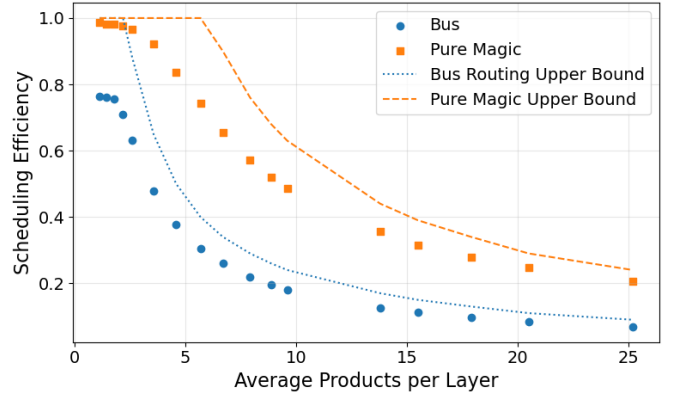


Fig. 11: Impact of products per layer (parallelism) in random circuits. The dots are the measured values and the dotted lines are the upper bounds computed from the availability of ready magic states.

In the first experiment, we varied the average Pauli products per layer across a wide range (from 1.13 to 25.19), to determine the impact on the Pure Magic scheduler. We expect increased parallelism to reduce the efficiency of scheduling, as it becomes harder to meet the demand for an increasing number of ready magic states. For 64 data qubits, the bus routing architecture has a total of 60 magic qubits; hence with an average cultivation time of 26 cycles, there are only 2.3 magic state qubits ready each cycle. For the Pure Magic architecture, there are 157 magic qubits, and thus 6 qubits would be ready each cycle if none were used for routing. This rate approaches the upper bound on the performance, as shown in Figure 11. The measured efficiencies for bus routing and Pure Magic scheduling are shown with dots and the dashed lines show the upper bounds on the efficiencies computed from the expected number of ready qubits. The actual efficiencies do not reach the upper bound because Pauli products in the same layer can sometimes require the same routing qubits, and hence cannot be co-scheduled. As expected, there is a larger gap between the upper bound and actual efficiency for Pure Magic scheduling because the magic state qubits get repurposed for routing.

One way to address the lack of ready magic qubits is to increase the number of qubits in the layout. However, this has the downside of increasing the volume, and hence potentially reducing overall efficiency. To understand the trade-off, we ran a series of experiments using Pure Magic scheduling with three levels of parallelism: low (1.42 average Pauli products per layer), medium (7.92 average Pauli products per layer) and high (25.13 average Pauli products per layer). For each level, we ran with 5 different layouts, from the most compact possible to a wide spread layout. The total number of qubits (including all ancilla and data) for the 64 qubit random circuits ranged from 153 to 1749.

Figure 12a shows how increasing the number of additional qubits increases the *parallel efficiency*, which is computed as

the minimum number of cycles (layers in the task graph), divided by the scheduled cycles. As expected, increasing available resources increases parallelism, until full parallelism is achieved for all circuits. However, the additional qubits can actually reduce the scheduling efficiency (Figure 12b) because that is related to volume (the product of the cycles and the number of logical qubits). For the low parallelism circuit, adding qubits always reduces the scheduling efficiency, whereas for medium parallelism, there is a distinct peak in scheduling efficiency just above the most compact layout, and for high parallelism, scheduling efficiency is slightly better across a wide range of mid-density layouts. This indicates that for most circuits, using additional resources beyond a certain level for routing and cultivation is not an effective strategy.

We have used a parameter of $\lambda = 0.00227$ for magic cultivation throughout, with a code distance of $d = 17$, which gives an average of 26 cycles for a qubit to cultivate magic state. This number will change for different code distances, and may also be improved with new ways to perform cultivation. We investigate the impact of the cultivation time on Pure Magic scheduling by running experiments with the three random circuits, low, medium and high. For each circuit, we test it with a varying parameter for the cultivation exponential, giving expected cultivation times of 1 to 64 cycles. The results are shown in Figure 13. For the low parallelism circuit, the cultivation time has little effect on the difference between Pure Magic and bus routing, except at very high cultivation times. By contrast, for high parallelism, every decrement in cultivation time gives Pure Magic an increase in efficiency over bus routing.

D. Comparison with Prior Work

This work is closest in nature to that of Silva et. al. [25]. In their paper, they present results with a set of specially generated benchmark circuits. For our work, we chose instead to use well-known benchmarks from the Benchpress suite. However, we have run our schedulers on the Silva et. al. benchmarks for comparison, using the versions they label “transpiled”. We present our scheduler performance compared to the results given in $E(N)$ column in Table 3 from Silva et. al. Specifically, we use our *bus routing* scheduler only, to get as close a comparison as possible to their results.

There are several limitations to this comparison. First, we do not know the exact layout used for their experiments, and thus we assume the compact layout (Figure 4a in Silva et. al.). Second, they assume magic distillation factories that provide magic state immediately. The equivalent in our case is to set the cultivation so it always takes only one cycle to complete. Finally, they do not use the top and bottom edges of the data qubits in their scheduling, and so we disable this in our scheduler.

The results of the comparison are show in Table III. Here we focus on the parallel efficiency, since we assume the layouts to be the same size for both approaches. In general, our results are close to theirs, and mostly somewhat better (higher parallel efficiency). This can likely be attributed to the differences

in the forest packing algorithms. In Silva et. al. they use a greedy approach where the next Pauli product to be scheduled is chosen at random. In our approach, we select the Pauli product with the smallest tree as the next to be scheduled. The benefits of this approach increase with the parallelism of the circuit, as can be seen for the RSC and Chain circuits.

TABLE III: Comparison with results from Table 3 in Silva et. al. The two righthand columns are parallel efficiencies.

Circuit	Qubits	Products per layer	T gates	Silva et. al.	Bus Routing
HH	4	1.26	20190	0.89	0.97
LiH	12	1.00	499956	1.00	1.00
HOH	14	1.00	1572334	1.00	1.00
Chain10	10	2.20	26094	0.73	0.93
Chain20	20	2.06	276383	0.75	0.95
Chain30	30	2.05	421462	0.77	0.92
Chain40	40	2.05	568238	0.76	0.96
Chain50	50	2.06	712165	0.76	0.96
TFSK10	10	1.26	405152	0.90	0.95
TFSK15	15	1.24	890287	0.90	0.92
Heisenberg5	5	1.22	177390	0.90	0.96
Heisenberg10	10	1.25	349330	0.90	0.99
Heisenberg20	20	1.35	707142	0.86	0.93
Heisenberg30	30	1.49	1023910	0.85	0.88
Heisenberg40	40	1.36	1394720	0.86	0.93
RSC3	9	2.07	16175	0.75	0.71
RSC5	25	2.86	216642	0.53	0.61
RSC7	49	3.03	396707	0.51	0.63

VI. DISCUSSION

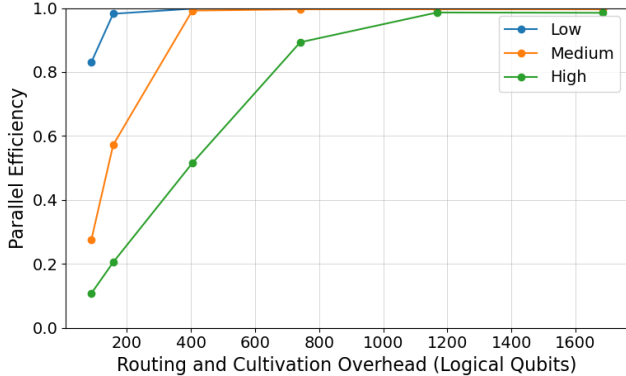
For the foreseeable future, fault tolerant quantum computers are likely to be constrained by the number of logical qubits they can provide. Thus, minimizing the ratio of ancilla to data qubits required for a computation becomes a measure of capability rather than performance. We expect dynamic scheduling techniques akin to Pure Magic to become widely deployed in QECC scheduling algorithms.

A. Increasing cultivation for higher fidelity

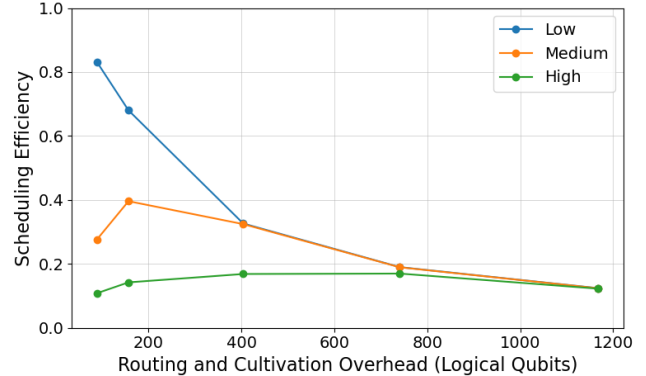
Our simulations assume a default expected cultivation time of 26 logical cycles (Section II-C). As seen in Figure 13, the volume improvements provided by Pure Magic become more pronounced as cultivation time increases. This is directly relevant for future large-scale fault tolerant quantum computing, because deeper algorithms demand lower logical error rates (Equation 1), which require higher-fidelity (and therefore longer) cultivation stages. Under these conditions, bus routing becomes increasingly hampered by long-tail cultivation events, while Pure Magic scheduling continues to amortize cultivation across a large pool of ancillary patches. Consequently, its benefits become even more significant in future-facing regimes where high-fidelity T states are unavoidable.

B. Compatibility with other codes and execution models

Although we present the Pure Magic architecture in the context of the surface code, the conceptual approach is not code specific. Any scheme in which magic states may be cultivated locally (e.g. with color codes and other codes [26],



(a) Parallel Efficiency



(b) Scheduling Efficiency

Fig. 12: Impact of increasing routing and cultivation overhead with additional logical qubits for random circuits with 64 data qubits and varying levels of parallelism (low, medium, high). Results are for Pure Magic scheduling.

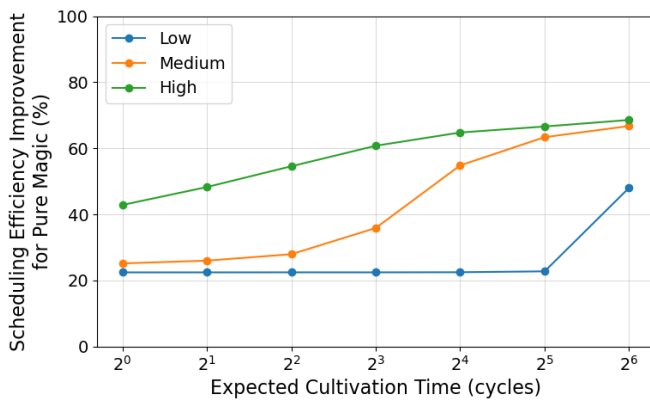


Fig. 13: Improvement in efficiency when using Pure Magic scheduling compared to bus routing for varying expected cultivation times. As cultivation time increases, Pure Magic hides more latency, resulting in greater relative improvements in efficiency.

[30]) could adopt a similar strategy. The key requirement is that ancillary space dedicated to routing be reallocated towards cultivation.

Similarly, execution models beyond Pauli Basis Computation (PBC) can also leverage the Pure Magic architecture. Direct gate execution frameworks, or hybrid PBC-gate models may exhibit higher intrinsic parallelism than the benchmarks studied here, suggesting that the relative advantage of Pure Magic could be larger in those contexts.

C. Comparing and benchmarking QECCs

In general, QECCs are compared based on their qubit overhead, error suppression capabilities, and suitability for different hardware architectures. For example, while surface codes are robust, they are often criticized for their high physical to logical qubit encoding overhead. Whenever a code is compared against surface codes, the comparison [29], [30] uses static logical qubit layouts with dedicated bus and magic

generation regions. This architecture has a fixed data to ancilla qubit ratio, and codes that use fewer physical qubits to encode a logical qubit tend to win against surface codes.

Pure Magic dynamic scheduling enables surface codes to save on logical qubits, providing an orthogonal way of reducing the ultimate count of physical qubits in the system. We argue that future code efficacy comparisons should take into account dynamic scheduling approaches and their ability to reduce the number of logical qubits involved in program execution. Because of these dynamics, comparisons must be made on *fully compiled* circuits mapped to hardware, rather than the gate level characteristics of a circuit.

D. Future directions

Our analysis makes several assumptions that highlight opportunities for future work:

- 1) *Y operators and twist defects.* We assume access to twist-based *Y* measurements, but with additional hardware support, Pauli products can be made twist free at the cost of increased execution time and volume [6]. Incorporating these costs may alter scheduling behavior.
- 2) *Planar connectivity.* We focus on architectures limited to 2D planar connectivities and lattice-surgery operations. Emerging demonstrations of transversal operations in small codes suggest that hybrid architectures may reduce routing pressure in ways complementary to Pure Magic [5].
- 3) *Static layouts.* All experiments assume a fixed layout. Dynamically reconfigurable logical layouts—where regions expand, contract, or move during execution—may synergize with Pure Magic. Long tail cultivation behavior could act as a heuristic for identifying high-quality patches, guiding dynamic data placement.

Our code is neither optimized nor parallelized. This could be a topic for future work, but currently the performance is adequate for this research. All the runs detailed here were carried out on a simple laptop (Intel i7-10875H processor),

and the median time taken over all the benchmarks was 40s, with the longest being 10 minutes (for Heisenberg 144).

VII. CONCLUSION

This paper has introduced Pure Magic scheduling, a novel approach to fault-tolerant quantum computation that dynamically repurposes magic-state cultivation qubits for routing operations, eliminating dedicated bus qubits while addressing magic-state preparation bottlenecks. Our experimental evaluation across 17 benchmark circuits demonstrates substantial improvements: Pure Magic achieves 19% to 223% better scheduling efficiency compared to traditional bus routing while requiring 19% to 80% fewer logical qubits. A key insight is that the probabilistic nature of magic-state cultivation becomes an advantage—by interrupting long-running cultivation for routing, the system naturally favors shorter cultivation times, reducing averages from 26 cycles to as few as 2.7 cycles.

The benefits scale with circuit parallelism, making Pure Magic particularly valuable for highly parallel quantum algorithms. Beyond immediate performance gains, this approach enables either faster computation with existing protocols or adoption of slower, higher-fidelity cultivation methods without proportional time penalties. Pure Magic represents a paradigm shift from static resource allocation to dynamic, demand-driven scheduling that we expect to generalize beyond surface codes to other quantum error-correcting codes relying on magic-state injection.

ACKNOWLEDGEMENTS

This work has been performed under DOE contract UC/DOE Prime Contract (No. DE-AC02-05CH11231).

REFERENCES

- [1] S. Aaronson and D. Gottesman, “Improved simulation of stabilizer circuits,” *Physical Review A*, vol. 70, no. 5, Nov. 2004. [Online]. Available: <http://dx.doi.org/10.1103/PhysRevA.70.052328>
- [2] BQSKit Development Team, “BQSKit: Berkeley quantum synthesis toolkit,” <https://github.com/BQSKit/bqskit>, 2024, accessed: 2025-01-16.
- [3] S. Bravyi and A. Kitaev, “Universal quantum computation with ideal Clifford gates and noisy ancillas,” *Physical Review A*, vol. 71, no. 2, p. 022316, 2005.
- [4] S. Bravyi, G. Smith, and J. A. Smolin, “Trading classical and quantum computational resources,” *Phys. Rev. X*, vol. 6, p. 021043, Jun 2016. [Online]. Available: <https://link.aps.org/doi/10.1103/PhysRevX.6.021043>
- [5] M. Cain, C. Zhao, H. Zhou, N. Meister, J. P. B. Ataides, A. Jaffe, D. Bluvstein, and M. D. Lukin, “Correlated decoding of logical algorithms with transversal gates,” *Physical Review Letters*, vol. 133, no. 24, p. 240602, 2024.
- [6] C. Chamberland and E. T. Campbell, “Universal quantum computing with twist-free and temporally encoded lattice surgery,” *PRX Quantum*, vol. 3, p. 010331, Feb 2022. [Online]. Available: <https://link.aps.org/doi/10.1103/PRXQuantum.3.010331>
- [7] A. G. Fowler and C. Gidney, “Low overhead quantum computation using lattice surgery,” 2018.
- [8] A. G. Fowler, M. Mariantoni, J. M. Martinis, and A. N. Cleland, “Surface codes: Towards practical large-scale quantum computation,” *Physical Review A*, vol. 86, no. 3, p. 032324, 2012.
- [9] C. Gidney, “How to factor 2048 bit rsa integers with less than a million noisy qubits,” 2025. [Online]. Available: <https://arxiv.org/abs/2505.15917>
- [10] C. Gidney, N. Shutty, and C. Jones, “Magic state cultivation: growing t states as cheap as cnot gates,” 2024. [Online]. Available: <https://arxiv.org/abs/2409.17595>
- [11] Y. Hirano and K. Fujii, “Locality-aware pauli-based computation for local magic state preparation,” 2025. [Online]. Available: <https://arxiv.org/abs/2504.12091>
- [12] D. Horsman, A. G. Fowler, S. Devitt, and R. Van Meter, “Surface code quantum computing by lattice surgery,” *New Journal of Physics*, vol. 14, no. 12, p. 123011, 2012.
- [13] A. Y. Kitaev, “Fault-tolerant quantum computation by anyons,” *Annals of Physics*, vol. 303, no. 1, pp. 2–30, 2003.
- [14] T. Kobori, Y. Suzuki, Y. Ueno, T. Tanimoto, S. Todo, and Y. Tokunaga, “Lsqca: Resource-efficient load/store architecture for limited-scale fault-tolerant quantum computing,” in *2025 IEEE International Symposium on High Performance Computer Architecture (HPCA)*. IEEE, Mar. 2025, p. 304–320. [Online]. Available: <http://dx.doi.org/10.1109/HPCA61900.2025.00033>
- [15] L. Kou, G. Markowsky, and L. Berman, “A fast algorithm for steiner trees,” *Acta informatica*, vol. 15, no. 2, pp. 141–145, 1981.
- [16] L. C. Lau, “Packing steiner forests,” in *International Conference on Integer Programming and Combinatorial Optimization*. Springer, 2005, pp. 362–376.
- [17] T. Leblond, C. Dean, G. Watkins, and R. Bennink, “Realistic cost to execute practical quantum circuits using direct clifford+t lattice surgery compilation,” *ACM Transactions on Quantum Computing*, vol. 5, no. 4, Oct. 2024. [Online]. Available: <https://doi.org/10.1145/3689826>
- [18] G. Lin and G. Xue, “On the terminal steiner tree problem,” *Information Processing Letters*, vol. 84, no. 2, pp. 103–107, 2002.
- [19] D. Litinski, “A game of surface codes: Large-scale quantum computing with lattice surgery,” *Quantum*, vol. 3, p. 128, Mar. 2019. [Online]. Available: <http://dx.doi.org/10.22331/q-2019-03-05-128>
- [20] A. Molavi, A. Xu, S. Tannu, and A. Albargouthi, “Dependency-aware compilation for surface code quantum architectures,” *Proc. ACM Program. Lang.*, vol. 9, no. OOPSLA1, Apr. 2025. [Online]. Available: <https://doi.org/10.1145/3720416>
- [21] P. D. Nation, A. A. Saki, S. Brandhofer, L. Bello, S. Garion, M. Treinish, and A. Javadi-Abhari, “Benchmarking the performance of quantum computing software for quantum circuit creation, manipulation and compilation,” *Nature Computational Science*, pp. 1–9, 2025.
- [22] J. O’Gorman and E. T. Campbell, “Quantum computation with realistic magic-state factories,” *Physical Review A*, vol. 95, no. 3, Mar. 2017.
- [23] R. Raussendorf and J. Harrington, “Fault-tolerant quantum computation with high threshold in two dimensions,” *Physical review letters*, vol. 98, no. 19, p. 190504, 2007.
- [24] K. Sahay, P.-K. Tsai, K. Chang, Q. Su, T. B. Smith, S. Singh, and S. Puri, “Fold-transversal surface code cultivation,” 2025. [Online]. Available: <https://arxiv.org/abs/2509.05212>
- [25] A. Silva, X. Zhang, Z. Webb, M. Kramer, C.-W. Yang, X. Liu, J. Lemieux, K.-W. Chen, A. Scherer, and P. Ronagh, “Multi-qubit lattice surgery scheduling,” Schloss Dagstuhl – Leibniz-Zentrum für Informatik, 2024. [Online]. Available: <https://drops.dagstuhl.de/entities/document/10.4230/LIPIcs.TQC.2024.1>
- [26] A. Steane, “Multiple particle interference and quantum error correction,” *Proceedings of the Royal Society A: Mathematical, Physical and Engineering Sciences*, vol. 452, 01 1996.
- [27] D. B. Tan, M. Y. Niu, and C. Gidney, “A sat scalpel for lattice surgery: Representation and synthesis of subroutines for surface-code fault-tolerant quantum computing,” in *2024 ACM/IEEE 51st Annual International Symposium on Computer Architecture (ISCA)*. IEEE, Jun. 2024, p. 325–339. [Online]. Available: <http://dx.doi.org/10.1109/ISCA59077.2024.00032>
- [28] Y. Vaknin, S. Jacoby, A. Grimsmo, and A. Retzker, “Efficient magic state cultivation on the surface code,” 2025. [Online]. Available: <https://arxiv.org/abs/2502.01743>
- [29] J. Viszlai, W. Yang, S. F. Lin, J. Liu, N. Nottingham, J. M. Baker, and F. T. Chong, “Matching generalized-bicycle codes to neutral atoms for low-overhead fault-tolerance,” 2024. [Online]. Available: <https://arxiv.org/abs/2311.16980>
- [30] T. J. Yoder, E. Schoute, P. Rall, E. Pritchett, J. M. Gambetta, A. W. Cross, M. Carroll, and M. E. Beverland, “Tour de gross: A modular quantum computer based on bivariate bicycle codes,” 2025. [Online]. Available: <https://arxiv.org/abs/2506.03094>